JBC RESEARCH ARTICLE

Exosomal miR-673-5p from fibroblasts promotes Schwann cell-mediated peripheral neuron myelination by targeting the TSC2/mTORC1/SREBP2 axis

Received for publication, October 22, 2021, and in revised form, February 6, 2022 Published, Papers in Press, February 11, 2022,
https://doi.org/10.1016/j.jbc.2022.101718

Yahong Zhao[*,‡], **Yunyun Liang**[‡], **Zhixin Xu, Jina Liu, Xiaoyu Liu, Jinyu Ma, Cheng Sun**[*], **and Yumin Yang**[*]

From the Key Laboratory of Neuroregeneration of Jiangsu and Ministry of Education; Co-innovation Center of Neurogeneration; NMPA Key Laboratory for Research and Evaluation of Tissue Engineering Technology Products, Nantong University, Nantong, China

Edited by Ronald Wek

Peripheral myelination is a complicated process, wherein Schwann cells (SCs) promote the formation of the myelin sheath around the axons of peripheral neurons. Fibroblasts are the second resident cells in the peripheral nerves; however, the precise function of fibroblasts in SC-mediated myelination has rarely been examined. Here, we show that exosomes derived from fibroblasts boost myelination-related gene expression in SCs. We used exosome sequencing, together with bioinformatic analysis, to demonstrate that exosomal microRNA miR-673-5p is capable of stimulating myelin gene expression in SCs. Subsequent functional studies revealed that miR-673-5p targets the regulator of mechanistic target of the rapamycin (mTOR) complex 1 (mTORC1) tuberous sclerosis complex 2 in SCs, leading to the activation of downstream signaling pathways including mTORC1 and sterol-regulatory element binding protein 2. *In vivo* experiments further confirmed that miR-673-5p activates the tuberous sclerosis complex 2/mTORC1/sterol-regulatory element binding protein 2 axis, thus promoting the synthesis of cholesterol and related lipids and subsequently accelerating myelin sheath maturation in peripheral nerves. Overall, our findings revealed exosome-mediated cross talk between fibroblasts and SCs that plays a pivotal role in peripheral myelination. We propose that exosomes derived from fibroblasts and miR-673-5p might be useful for promoting peripheral myelination in translational medicine.

Myelination is a complicated biological process which involves the formation of a myelin sheath around nerve cell axons so as to insulate them from the surroundings and thus favoring electrical impulses passing along the axon. Schwann cells (SCs) and oligodendrocytes are the two main glial cells responsible for myelination in the peripheral nervous system and central nervous system (CNS). Myelin membranes are mainly composed of proteins and lipids, including cholesterol, galactosphingolipids, and saturated long-chain fatty acids, which account for at least 70% of the dry weight of myelin membranes (1). Defects in lipid synthesis in SCs or oligodendrocytes are often associated with various neuropathies such as Smith-Lemli-Opitz-syndrome, Refsum's disease, and Tangier disease (2–4). In accordance, any interruption in lipid synthesis has been shown to impair the structure and function of myelin in both the peripheral nervous system and CNS (5–12).

Fibroblasts are widely distributed in many types of tissues, and their main task is to synthesize and organize matrix proteins (13, 14). Fibroblasts in normal adult tissues are generally quiescent. However, as they can be activated under specific conditions, such as wound healing, tissue fibrosis, and cancer progression, fibroblasts play key roles in tissue repair, scar formation, and tumor metastasis (15–18). In peripheral nerves, SCs and fibroblasts are the two main types of cells, accounting for 45% and 25%, respectively (19). Moreover, similar to SCs, fibroblasts are derived from neural crest stem cells (20). Most recently, fibroblasts were identified in peripheral nerves of neonatal rats by cell population identification using single-cell transcriptomics (21). Although fibroblasts have been considered as resident cells in the peripheral nerves for a long time, to date, the precise functions of fibroblasts are not well understood. It has been shown that in cut nerves, ephrin-B/EphB2 signaling between fibroblasts and SCs directs cell sorting and guides the regrowth of axons across the wound (22). Exosomes are endosome-derived small extracellular vesicles with diameters of 40 to 150 nm (23). By trafficking RNA, DNA, proteins, and lipids, exosomes have been shown to play various essential roles, especially in cell–cell interaction (24–26). Due to the same niches for fibroblasts and SCs in peripheral nerves, we predicted that fibroblast exosomes might be a key transducer for regulating behaviors of SC such as myelination.

In the present study, we examined the potential interaction between fibroblasts and SCs, and found that fibroblast-derived exosomes promote myelin gene expression in SCs. Exosome sequencing followed by bioinformatics analysis revealed that exosomal miR-673-5p is a key molecule for transducing promoted myelin gene expression in SCs. Furthermore, it was noted that miR-673-5p targets the axis of TSC2/ mechanistic

‡ These authors contributed equally for this work.
* For correspondence: Yumin Yang, yangym@ntu.edu.cn; Cheng Sun, suncheng1975@ntu.edu.cn; Yahong Zhao, zhaoyh108@ntu.edu.cn.

target of the rapamycin complex 1 (mTORC1)/SREBP2 in SCs and thus stimulates cholesterol synthesis for myelin formation. Together, our study revealed a cross talk between fibroblasts and SCs in peripheral nerve myelination and demonstrated that fibroblast exosomal miR-673-5p is a pivotal molecule in this process.

Results

Peripheral nerve fibroblasts–derived exosomes promote myelin gene expression in SCs

Peripheral myelination in rats starts after birth and is accomplished in 2 weeks (27). To explore the potential roles of fibroblasts in peripheral myelination, we first measured the amount of fibronectin synthesized by fibroblasts during the developmental myelination process in sciatic nerves. As shown in Figure 1*A*, prolyl 4-hydroxylase subunit beta and fibronectin expression in rat sciatic nerves was reduced gradually along with myelin maturation, suggesting that fibroblasts switched from activation to silence in this process. Moreover, peripheral nerve fibroblasts have been shown to play important roles in various biological events to maintain proper physiological functions of peripheral nerves (22, 28–30). Therefore, we speculated that fibroblasts may also play key roles in peripheral myelination. Next, we isolated primary fibroblasts from the rat sciatic nerves to address this prediction. CD90 being a well-documented marker of fibroblasts, an anti-CD90 antibody was employed for fibroblast identification (31). Immunofluorescence data confirmed that the purity of cultured fibroblasts was above 95% (Fig. S1*A*). Myelination is an essential process for the peripheral nerves that is accomplished by SCs (1). We examined the potential roles of fibroblasts in myelination by SCs. Primary rat SCs were treated with cell culture medium from fibroblasts, and myelin gene expression was examined. Dibutyryl cyclic AMP (db-cAMP) has been defined as a second messenger in the promotion of myelination (32); thus, it was used as a positive control. The results showed that the conditioned medium treatment greatly stimulated myelin gene expression, including *Oct6*, *Krox20*, and *Pmp22* (Fig. 1*B*). However, the conditioned medium from GW4869-treated fibroblasts showed no such effects (Fig. 1*B*). Since GW4869 is a potent inhibitor of exosome secretion (33), we predicted that exosomes in the medium may play key roles in myelin gene expression.

Next, we prepared exosomes from peripheral nerve fibroblasts and examined their effects on myelin gene expression in SCs. Nanoparticle tracking analysis showed that while the exosome diameter was approximately 145.8 nm, the vesicles from GW4869-treated fibroblasts measured approximately 167.0 nm in diameter (Fig. S1, *B* and *C*). Moreover, the vesicle density was markedly reduced in the presence of GW4689 (Fig. S1, *B* and *C*), indicating that it is capable of repressing exosome secretion. Additionally, we analyzed the prepared exosomes by transmission electron microscopy (TEM). The captured TEM images revealed that the prepared exosomes had cup-like shapes (Fig. 1*C*), a classical feature of exosomes (23, 34). To further confirm the purity of exosomes, we measured CD9 and CD63, the two reliable markers of exosomes (23, 24). Data of Western blot showed that compared to the whole-cell lysates, CD9 and CD63 were highly expressed in the prepared exosomes (Fig. 1*D*). Calnexin is an endoplasmic reticulum resident protein, that is often used as a negative marker of exosomes (35). In accordance, the expression of Calnexin in exosomes was relatively low (Fig. 1*D*). Actin was presented in both exosomes and whole-cell lysates (Fig. 1*D*). Moreover, the prepared fibroblast-derived exosomes could be internalized by SCs (Fig. 1*E*). As expected, fibroblast exosomes promoted myelin gene expression (Fig. 1*F*). To further confirm these observations, we performed immunofluorescence analysis for *Krox20*, a key transcription factor for myelin gene expression (36). The results showed that *Krox20* expression in SCs was remarkably increased by exosomes (Fig. S2). Collectively, the data clearly indicate that peripheral fibroblast exosomes are capable of inducing myelin gene expression in SCs, suggesting their potential roles in peripheral myelination.

mTORC1 is targeted by fibroblast exosomal miRNAs for transducing the promotion effects on myelin gene expression in SCs

In general, exosomes contain several substances, including nucleic acid (DNA, RNA), proteins, lipids, amino acids, and some other metabolites (37). Nevertheless, numerous studies have shown that miRNAs are considered the main factors that transduce various physiological functions of exosomes (38–43). Therefore, we focused our interest on exosomal miRNAs, and with this aim, miRNA sequencing was performed, and a total of 490 miRNAs were identified (Table S1). Functional annotation revealed that these miRNAs have multiple functions (Fig. 2*A*). We also analyzed the main biological events in SCs using clustering coefficient analysis (https://www.ebi.ac.uk) (Fig. 2*B*). Notably, the mTOR signaling pathway was presented in both bioinformatic analyses. mTOR, a serine/threonine protein kinase, plays a pivotal role in a number of fundamental cellular events, ranging from protein synthesis to autophagy (44). mTOR has two distinct protein complexes: mTORC1 and mTOR complex 2 (45). It has been demonstrated that mTORC1 is required for proper peripheral myelination (6, 8, 46–48). Hence, in the subsequent experiments, we tested whether the mTORC1 pathway was responsible for the increased myelin gene expression in SCs induced by fibroblast exosomes. Toward this end, SCs were treated with exosomes and rapamycin, an allosteric inhibitor of mTORC1 (49). Our data showed that rapamycin repressed myelin gene expression in SCs, and the stimulated myelin gene expression induced by exosomes was completely counteracted by rapamycin (Fig. 2, *C*–*F*). These results strongly suggest that mTORC1 is a key node for transducing the effects of fibroblast exosomes on myelination in SCs.

Exosomal miR-673-5p targets Tsc2 to promote myelin gene expression in SCs

To identify which miRNA in exosomes activates mTORC1 and thus stimulates myelin gene expression in SCs, we

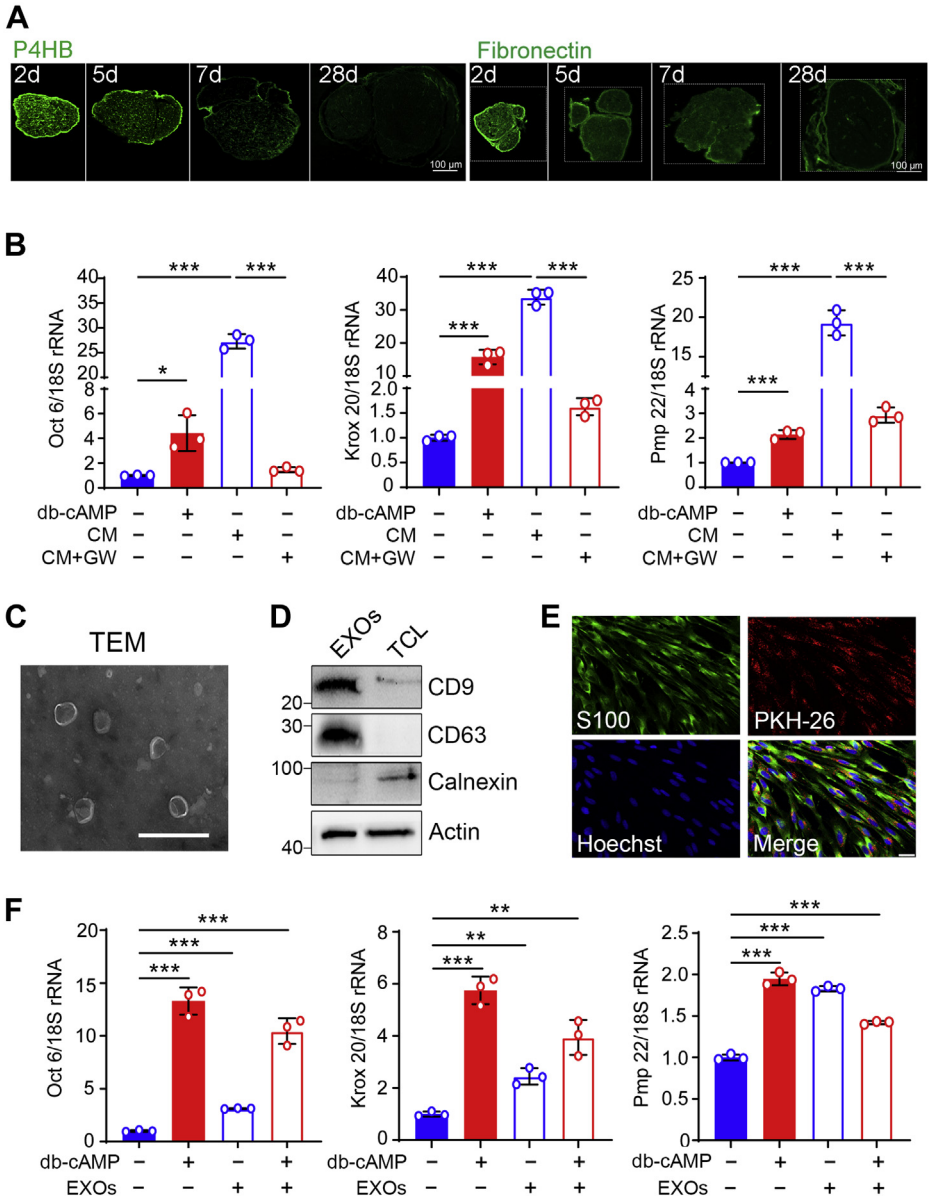

Figure 1. Exosomes derived from fibroblasts improve myelin gene expression in SCs. *A*, fibroblasts in the development of sciatic nerves in rats. The transections of sciatic nerves from rats at different ages were subjected to immunofluorescence analysis by using anti-prolyl 4-hydroxylase subunit beta (P4HB) or anti-fibronectin antibody. Scale bar = 100 μm. *B*, fibroblast culture medium promotes myelin gene expression in SCs. SCs were treated with the culture medium from fibroblasts or GW4869-treated fibroblasts. 1 mM of db-cAMP was used as a positive control. *Oct 6*, *Krox 20*, and *Pmp 22* expressions were analyzed by quantitative real-time PCR (qRT-PCR), and 18S rRNA was used as an internal control. *C*, transmission electron microscopy analysis of fibroblast exosomes. Scale bar = 500 nm. *D*, Western blot analysis showing exosome markers CD9 and CD63. Calnexin was used as a negative control. Actin was used as loading control. *E*, fluorescent microscopy analysis showing fibroblasts-derived exosomes could be internalized by SCs. Exosomes derived from fibroblasts were labeled by PKH-26 and co-cultured with SCs for 24 h. SCs were stained by S100 in *green* and the labeled exosomes were in *red*. Hoechst was used to stain the nucleus. Scale bar = 25 μm. *F*, fibroblast exosomes stimulate myelin gene expression in SCs. Exosomes from fibroblasts were prepared and used for treating SCs for 24 h. *Oct 6*, *Krox 20*, and *Pmp 22* expressions were analyzed by qRT-PCR. 18S rRNA was used as an internal control. Data are expressed as means ± SD. Statistical significance was analyzed by one-way ANOVA test. *$p < 0.05$, **$p < 0.01$, ***$p < 0.001$. CM, culture medium; db-cAMP, dibutyryl cyclic AMP; EXOs, exosomes; GW, GW4689; SCs, Schwann cells; TCL, total cell lysates; TEM, transmission electron microscopy.

analyzed the network of mTORC1 (Fig. 3*A*). Tuberous sclerosis complexes 1 and 2 (TSC1/2) are widely accepted as negative regulators of mTOR (44, 50). Furthermore, based upon the mTOR signaling pathway, we carried out regulatory network analysis and tried to find the key miRNAs. The potential target genes of differentially expressed miRNAs in SCs were predicted using an online database of miRNA targets (http://www.ebi.ac.uk/ena/ and http://www.targetscan.org/vert_72/). By combining the network analysis and the predicted miRNAs, we found that fibroblast exosomal miR-665, miR-3072, miR-667-3p, and miR-673-5p are potential miRNAs that target TSC2. We further quantified these miRNAs in SCs treated with the prepared exosomes and found that the amount of all the tested miRNAs was increased by the exosomes (Fig. 3*B*). Moreover, we analyzed the basal levels of these miRNAs in culture medium of SCs. The results showed

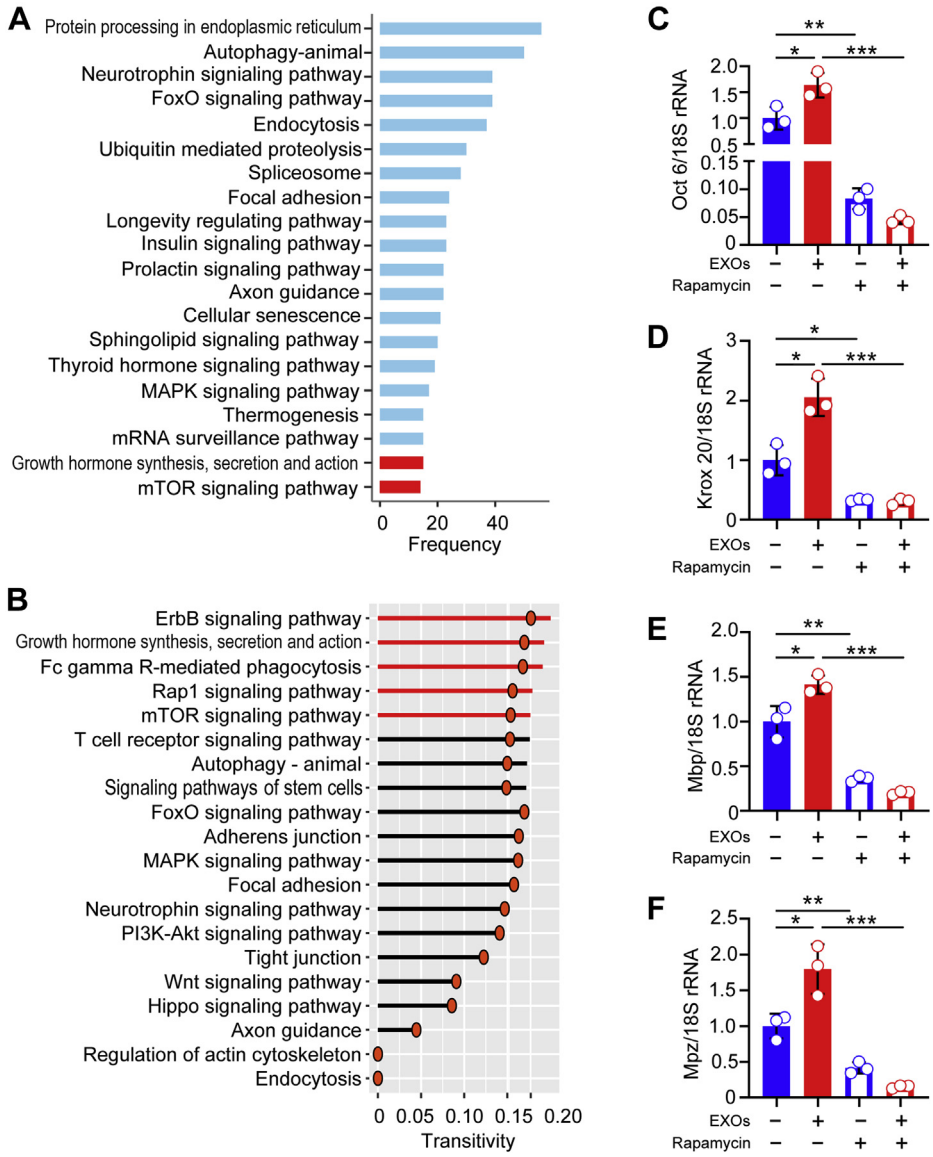

Figure 2. mTORC1 was involved in fibroblast exosome promoted myelin gene expression in SCs. *A*, functional annotations of miRNAs in exosomes derived from fibroblasts. Gene ontology analysis indicated the most significantly enriched canonical signaling pathways. For each pathway, the genes targeted by exosomal miRNAs are separated into two groups, myelin-related (*red*) or nonrelated (*blue*). *B*, the clustering coefficient analysis showing the most significantly enriched canonical signaling pathways in SCs. The pathways labeled in *red* are associated with myelination in SCs. *C–F*, the exosome-stimulated myelin gene expression in SCs was suppressed by rapamycin. SCs were treated with exosomes and rapamycin (2.5 mM) as indicated for 24 h. *Oct 6*, *Krox 20*, *Mbp*, and *Pmp 22* expressions were analyzed by qRT-PCR, 18S rRNA was used as an internal control. Data are expressed as means ± SD. Statistical significance was analyzed by one-way ANOVA test. $^{*}p < 0.05$, $^{**}p < 0.01$, $^{***}p < 0.001$. EXOs, exosomes; mTORC1, mechanistic target of the rapamycin complex 1; qRT-PCR, quantitative real-time PCR.

that the expression of miR-665, miR-3072, miR-667-3p, and miR-673-5p was rather low, especially for miR-3072 and miR-673-5p (Fig. 3*C*).

We then explored whether TSC2 affects myelin gene expression. For this, SCs were successfully transfected with the plasmid expressing *Tsc2* by electroporation, as evidenced by the robust increase in *Tsc2* gene expression (Fig. 4*A*). *Krox20* expression was stimulated by db-cAMP; however, the induced expression was largely abolished by TSC2 (Fig. 4*A*). Concurrently, the possible involvement of TSC1 in this process was also examined. Unlike TSC2, we found that *Krox20* expression was not altered by TSC1 (Fig. 4*B*). Moreover, TSC2 knockdown by siRNA further increased *Krox20* expression in SCs (Fig. 4, *C* and *D*). These data strongly imply that TSC2, other than TSC1, negatively regulates myelin gene expression in SCs. To further examine which exosomal miRNA targets TSC2, we synthesized the mimic and inhibitor for each miRNA including miR-665, miR-667-3p, miR-3072, and miR-673-5p. Of these, only the miR-673-5p mimic repressed *Tsc2* expression, and its inhibitor enhanced *Tsc2* expression (Fig. 4*E*). Therefore, miR-673-5p was considered as a functional molecule in fibroblast exosomes targeting *Tsc2* and thus transduces the promotion effects on myelin gene expression in SCs. To further verify this, we treated primary SCs with miR-673-5p mimic or inhibitor. It was noted that the db-cAMP-induced *Krox20* expression was markedly repressed

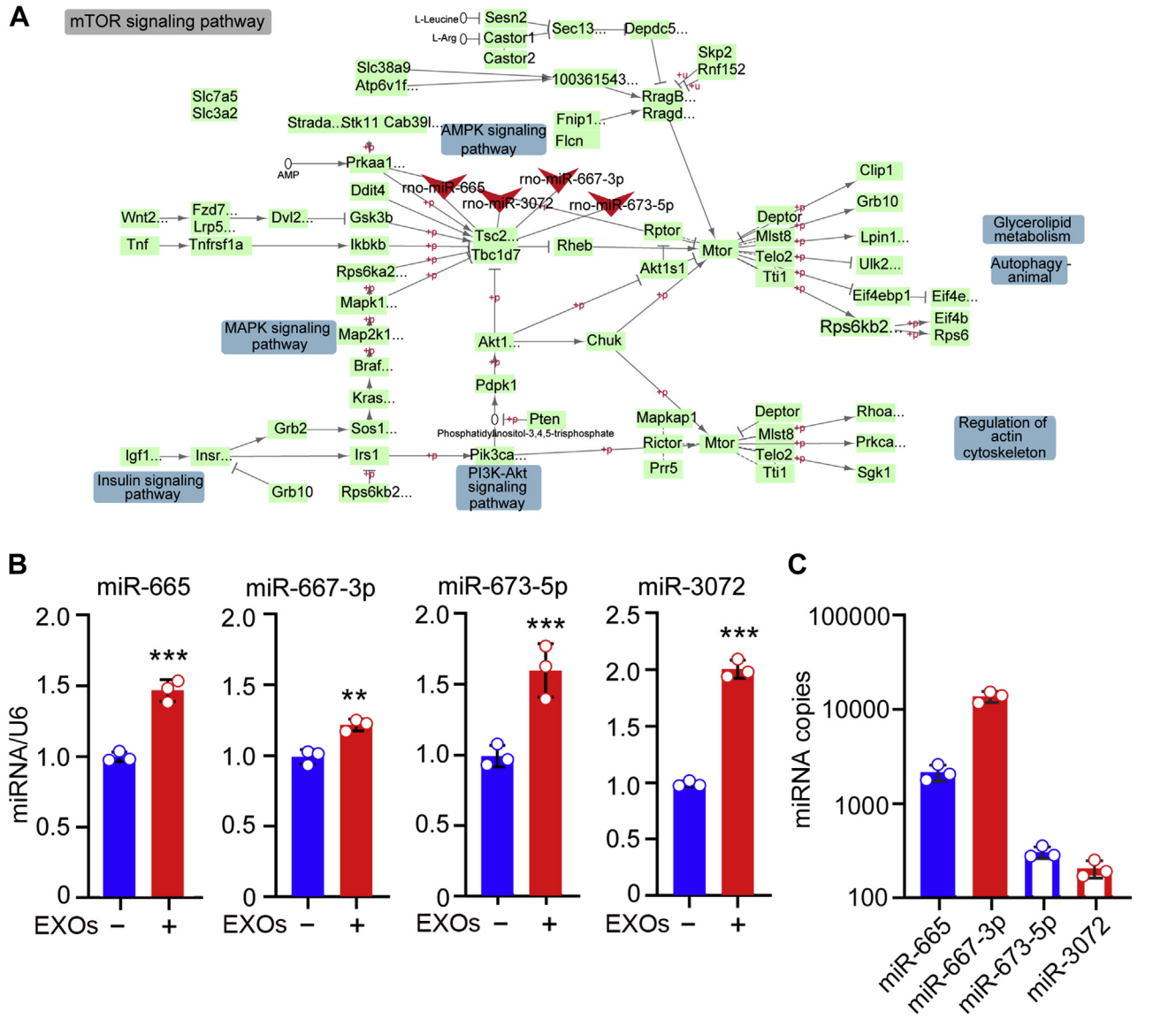

Figure 3. The axis of TSC2/mTORC1 was potentially targeted by the exosomal miRNAs. *A*, the mTOR signaling pathway in KEGG pathway analysis. TSC2 is a negative regulator for mTOR. Bioinformatics analysis showing the exosomal miR-665, miR-667-3p, miR-673-5p, and miR-3072 are potential regulators by targeting TSC2. *B*, exosomes from fibroblasts transfer miR-665, miR-667-3p, miR-673-5p, and miR-3072 in SCs. SCs were treated with exosomes for 24 h, and miRNA expression was analyzed by qRT-PCR. U6 was used as an internal control. *C*, a concentration of 10^9 copies/μl cel-miR-39 was added in culture medium of SCs. Exosomes were extracted by the exoRNeasy method. The expression of miR-665, miR-667-3p, miR-673-5p, and miR-3072 in culture medium of SCs. Data are expressed as means ± SD. Statistical significance was analyzed by Student's *t* test. *$p < 0.05$, **$p < 0.01$, ***$p < 0.001$. EXOs, exosomes; mTORC1, mechanistic target of the rapamycin complex 1; qRT-PCR, quantitative real-time PCR; SCs, Schwann cells; TSC, tuberous sclerosis complex.

by the inhibitor; on the contrary, the mimic further increased *Krox20* expression (Fig. 4*F*). TSC2 completely abolished the increased *Krox20* expression induced by miR-673-5p (Fig. 4*G*). Inhibition of mTORC1 by rapamycin also resulted in similar changes in *Krox20* expression (Fig. 4*H*). Together, these data indicate that by targeting *Tsc2*, miR-673-5p is responsible for the increased myelin gene expression in SCs induced by fibroblast exosomes.

miR-673-5p promotes lipid synthesis via *TSC2/mTORC1/SREBP2 in sciatic nerves*

Sterol-regulatory element binding proteins (SREBP1/2) are the two main downstream targets of mTORC1 (6, 7, 51). Hence, we analyzed SREBP1/2 and their target genes in the sciatic nerves. The results showed that miR-673-5p increased the expression of *Srebp1* in the sciatic nerves at 11 days posttreatment, and a reduction was observed at 15 days (Fig. 5*A*). At other time points, *Srebp1* expression was not altered by miR-673-5p (Fig. 5*A*). As a consequence, the downstream effectors of SREBP1, such as *Acc1*, *Fasn*, and *Acly*, were also not significantly altered by miR-673-5p (Fig. 5*A*). As for *Srebp2*, its expression was markedly increased by miR-673-5p at 2-, 7-, 11-, and 15-days posttreatment (Fig. 5*A*). *Hmgcr*, a target gene of SREBP2, was enhanced by miR-673-5p at 2-, 7-, and 11-days posttreatment (Fig. 5*A*). To further confirm that *Srebp2* is a downstream effector of miR-673-5p, we treated SCs with miR-673-5p mimic and inhibitor and examined *Srebp2*

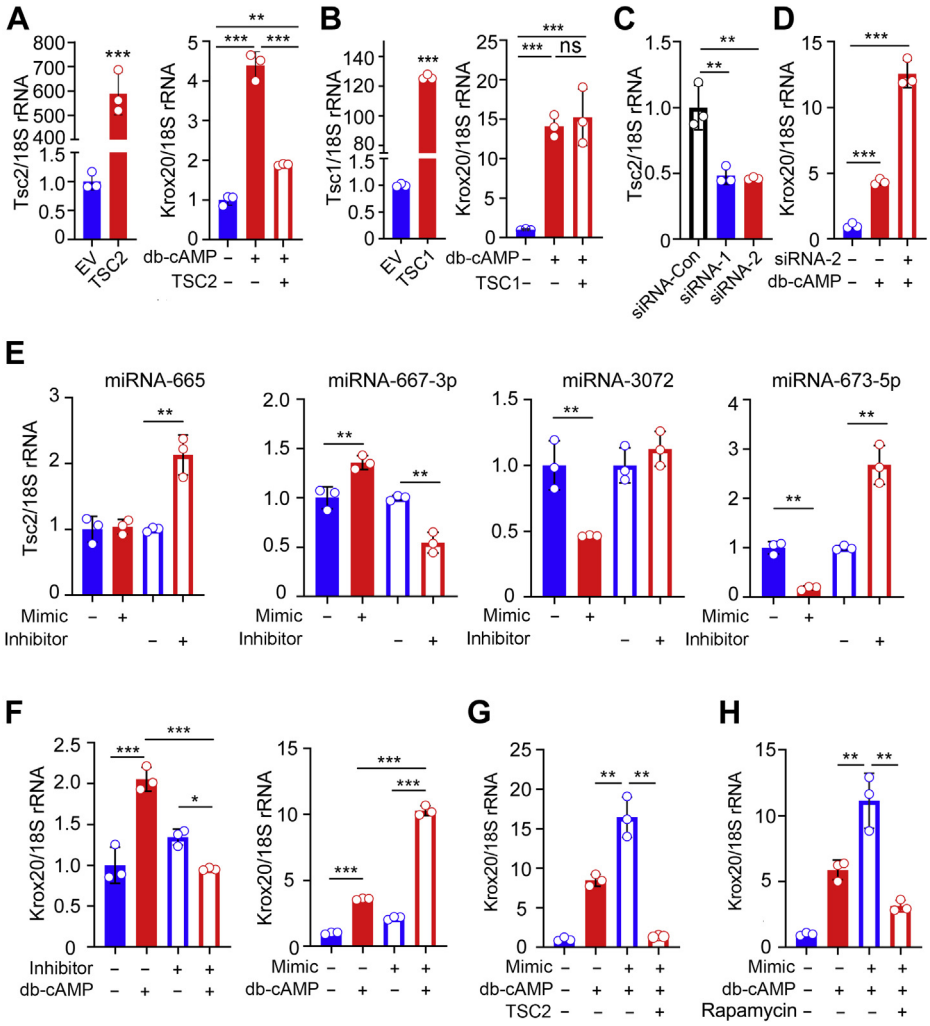

Figure 4. TSC2 is targeted by exosomal miR-673-5p and negatively regulates myelin gene expression in SCs. *A*, effects of TSC2 on *Krox20* expression. SCs were transfected with the plasmid expressing *Tsc2*. Twelve hours posttransfection, cells were treated with db-cAMP for additional 24 h. *B*, effects of TSC1 on *Krox20* expression. SCs were transfected with the plasmid expressing *Tsc1* by electroporation. Twelve hours posttransfection, cells were treated with 1 mM of db-cAMP for additional 24 h. *C*, *Tsc2* knockdown. SCs were transfected with *Tsc2* siRNA by electroporation. Seventy-two hours posttransfection, cells were harvested for analyzing *Tsc2* expression. *D*, *Tsc2* knockdown promotes myelin gene expression. SCs were transfected with *Tsc2* siRNA by electroporation. Forty-eight hours posttransfection, cells were treated with 1 mM db-cAMP for additional 24 h. *E*, effects of miR-665, miR-667-3p, miR-673-5p, and miR-3072 mimics and inhibitors on *Tsc2* expression. SCs were transfected with mimic or inhibitor for each miRNA for 24 h. *F*, effects of miR-673-5p mimic and inhibitor on *Krox20* expression. SCs were transfected with miR-673-5p mimic or inhibitor for 24 h followed by the treatment with 1 mM of db-cAMP as indicated for additional 24 h. *G*, TSC2 abolishes *Krox20* expression induced by miR-673-5p. SCs were transfected with the plasmid expressing *Tsc1* and miR-673-5p mimic by electroporation as indicated. Twelve hours posttransfection, cells were treated with 1 mM db-cAMP for additional 24 h. *H*, rapamycin represses *Krox20* expression induced by miR-673-5p. SCs were transfected with miR-673-5p mimic for 12 h, and then cells were treated with 1 mM db-cAMP and 2.5 mM rapamycin for additional 24 h. The mRNA levels of *Tsc1*, *Tsc2*, and *Krox20* were analyzed by qRT-PCR and 18S rRNA was used as an internal control. Data are expressed as means ± SD. Statistical significance was analyzed by one-way ANOVA test. $*p < 0.05$, $**p < 0.01$, $***p < 0.001$. db-cAMP, dibutyryl cyclic AMP; EV, empty vector; qRT-PCR, quantitative real-time PCR; SCs, Schwann cells; TSC2, tuberous sclerosis complex 2.

expression. The miR-673-5p mimic greatly enhanced miR-673-5p expression in SCs (Fig. 5*B*). As expected, *Srebp2* was increased by the mimic, and its expression was repressed by the inhibitor (Fig. 5*B*). Moreover, we also analyzed 3-hydroxy-3methylglutaryl coenzyme A (*Hmgcr*), a downstream target of SREBP2 (52). Similar changes in *Hmgcr* induced by the miR-673-5p mimic or inhibitor were observed (Fig. 5*B*).

Since *Srebp2* and *Hmgcr* are responsible for *de novo* cholesterol biosynthesis (53–55), we predicted that cholesterol and related lipids in sciatic nerves might be altered by miR-673-5p. To address this, we performed lipidomics analysis of the sciatic nerves treated with miR-673-5p agomir. The lipidomics data showed that a number of lipids, including phosphatidylcholine, phosphatidylethanolamine, phosphatidylserine, and diacyl glycerol, were increased by the miR-673-5p agomir (Fig. 6, *A* and *B*). Of these, phosphatidylcholine, phosphatidylethanolamine, and phosphatidylserine are the main constituents involved in myelin sheath formation (56). Therefore, we calculated the relative contents of these lipids based on lipidomics data and found that these three components were enhanced by miR-673-5p agomir in both P7 and P11 rats (Fig. 6, *C* and *D*). We also examined cholesterol levels in the sciatic nerves. As shown in Figure 6*E*, in rats treated with the miR-673-5p agomir, the level of cholesterol in the sciatic nerves was stimulated.

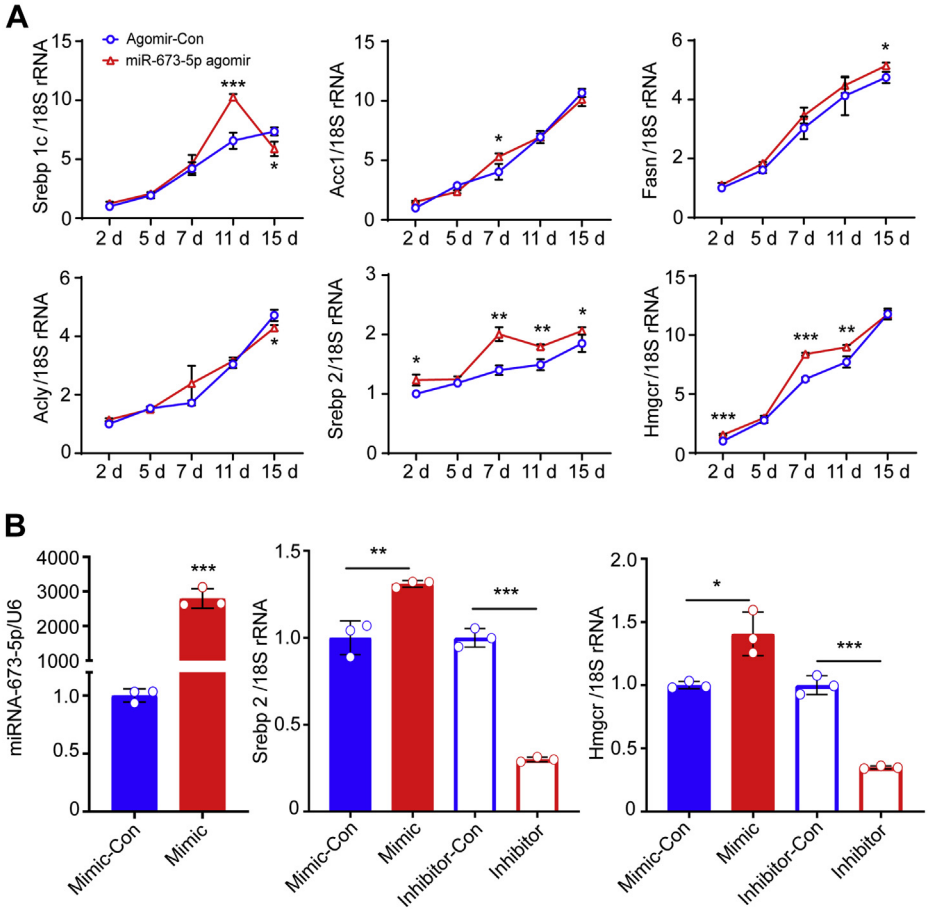

Figure 5. miRNA-673-5p targets TSC2 and stimulates mTORC1. *A*, qRT-PCR analysis of genes related to mTORC1 signaling pathway. Sciatic nerves were isolated from P2, P5, P7, P11, and P15 rats treated with agomir control or miR-673-5p agomir. *B*, miR-673-5p positively regulates *Srebp2* and *Hmgcr*. SCs were transfected with miR-673-5p mimic or inhibitor for 48 h. Expression of *Srebp2* and *Hmgcr* was analyzed by qRT-PCR, and 18S rRNA was used as an internal control. Data are expressed as means ± SD. Statistical significance was analyzed by Student's *t* test. $*p < 0.05$, $**p < 0.01$, $***p < 0.001$. mTORC1, mechanistic target of the rapamycin complex 1; qRT-PCR, quantitative real-time PCR; SCs, Schwann cells; TSC2, tuberous sclerosis complex 2.

miR-673-5p agomir promotes sciatic nerve myelination in newborn rats

Our data showed that fibroblast exosomal miR-673-5p targets *Tsc2*, leading to the activation of mTORC1 and its downstream effectors, such as SREBP2 and HMGCR. *Srebp2* is a major transcription factor that controls the expression of cholesterol and lipid biosynthetic genes (53). HMGCR is a rate-limiting enzyme in the cholesterol biosynthetic pathway. Hence, we proposed that fibroblast-derived exosomal miR-673-5p inhibits *Tsc2* in SCs, leading to the activation of mTORC1 and its downstream targets such as *Srebp2* and *Hmgcr*. Consequently, the biosynthesis of cholesterol and its related lipids in SCs is promoted, which may then facilitate myelination in the sciatic nerves. To confirm this, neonatal rats were administered with synthesized miR-673-5p agomir. The sciatic nerves were sampled at different time points, such as 2, 5-, 7-, 11-, and 15-days postinjection. As a substrate of miR-673-5p, *Tsc2* expression was downregulated by the miR-673-5p agomir (Fig. 7*A*). Moreover, *Oct6* and *Krox20* were stimulated by the miR-673-5p agomir (Fig. 7*A*). The expression of myelin genes such as *Mpb*, *Mpz*, and *Pmp22* were increased until 11 days postinjection and decreased to some extent thereafter (Fig. 7*A*). Furthermore, we analyzed KROX20 and MPZ expression in sciatic nerves using immunofluorescence. The results showed that both KROX20 and MPZ were increased by miR-673-5p agomir at 2-, 5-, 7-, and 11-days postinjection (Fig. 7, *B* and *C*). TEM images revealed that the myelin sheath in sciatic nerves became thicker in miR-673-5p agomir–treated animals, which was further confirmed by the decreased g-ratio values (Fig. 8, *A* and *B*). Myelinated axons were also increased by miR-637-5p agomir (Fig. 8*C*). Meanwhile, we also treated newborn rats with fibroblast-derived exosomes. Similar to miR-673-5p agomir, the treatment of exosomes greatly promoted myelination in sciatic nerves; for example, the thickness of myelin sheath, the diameter of myelinated fibers, and the numbers of myelin lamellae were all increased by exosomes (Fig. 9, *A* and *B*). These data clearly indicate that fibroblast-derived exosomes have a positive impact on peripheral myelination, in which exosomal miR-673-5p is a key molecule.

Discussion

In peripheral nerves, fibroblasts are the second resident cells after SCs (19). However, till date, the precise role of fibroblasts in proper functioning of peripheral nerves is unclear. In the

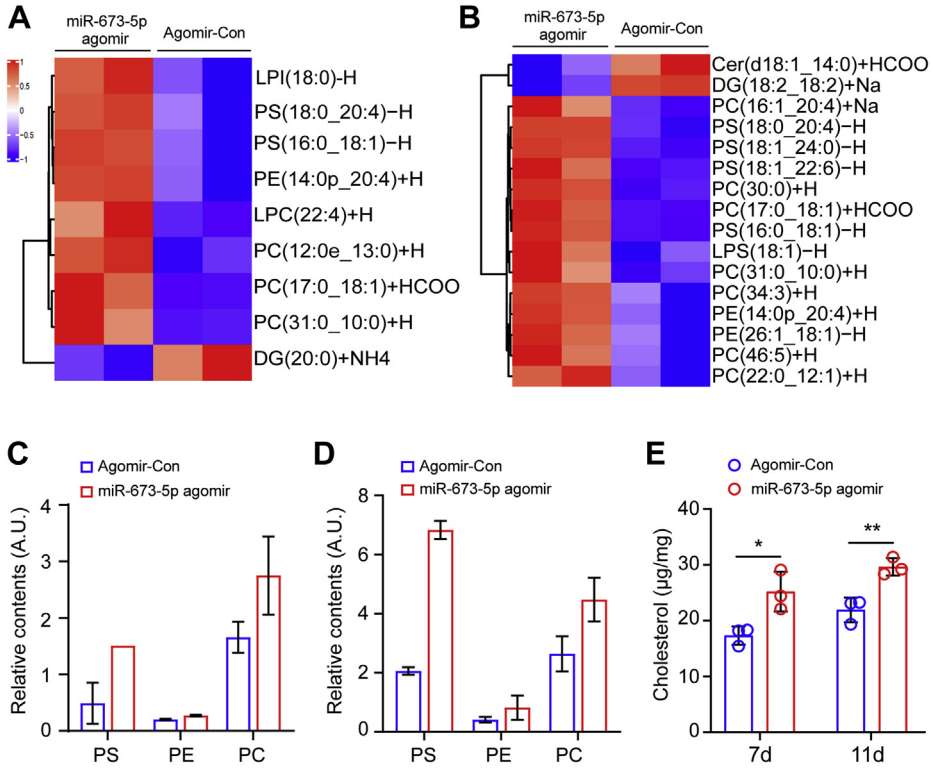

Figure 6. miRNA-673-5p potentiates lipid constituents in the sciatic nerves. *A* and *B*, heatmap showing miRNA-673-5p agomir affects lipid constituents. Newborn rats (P1) were received miRNA-673-5p agomir *via* hypodermic injection. The sciatic nerves were collected at P7 (*A*) and P11 (*B*) and subjected to lipidomics analysis. *C* and *D*, the main lipids in myelin sheath were enhanced by miR-673-5p agomir. The relative contents of phosphatidylcholine, phosphatidylethanolamine, and phosphatidylserine in the sciatic nerves from P7 (*C*) and P11 (*D*) were obtained from lipidomics data. A.U. means arbitrary units. *E*, cholesterol contents in the sciatic nerves were increased by miR-673-5p agomir. Data are expressed as means ± SD. Statistical significance was analyzed by Student *t* test. $^{*}p < 0.05$, $^{**}p < 0.01$. PC, phosphatidylcholine; PE, phosphatidylethanolamine; PS, phosphatidylserine.

present study, we identified a cross talk between fibroblasts and SCs for regulating peripheral myelination, which is mediated by exosomes derived from fibroblasts. Fibroblast exosomal miR-673-5p targets *Tsc2*, leading to the activation of mTORC1 and its downstream effector SREBP2 in SCs. As a consequence, fatty acid and cholesterol synthesis in SCs was stimulated, which in turn favor the myelin sheath formation.

Fibroblasts are the major cells responsible for constructing the extracellular matrix by producing matrix proteins, including collagen, laminin, tenascin, nidogen, fibronectin, and water-holding glycoproteins (13, 14). There are many types of fibroblasts in mammals based on differences in anatomical sites and gene expression profiles (13, 14). Each type of fibroblast has its own distinct fundamental role in various physiological events, such as organ formation, wound healing, and pathological progression (13, 14). Although fibroblasts account for 25% of peripheral nerve resident cells (19), little is known about their roles in the developmental processes of peripheral nerves. Peripheral nerve resident fibroblasts have been shown to direct SC sorting *via* the EphB signaling pathway in peripheral nerve regeneration (22). In addition, they observed that fibroblasts undergo a transformation from quiescent stages into activated forms in peripheral nerve injury (22). In line with these findings, we also found that fibroblast activation occurred synchronously with the developmental process of peripheral nerve myelination, which strongly imply fibroblasts may play a role in this process. Indeed, our subsequent experiments revealed that fibroblast-derived exosomes stimulate myelin gene expression and potentiate fatty acid and cholesterol synthesis in SCs and thus favoring peripheral nerve myelination.

mTOR is a serine threonine protein kinase, that includes two distinct subtypes, mTORC1 and mTOR complex 2. Of these, mTORC1 is responsible for mRNA translation and biosynthesis of lipids, pyrimidines, and purines (57–59), all of which are considered anabolic reactions. Given that myelination is an anabolically demanding process, mTORC1 may be involved in the myelination. Indeed, genetic disruption of mTORC1 in SCs or oligodendrocytes impairs myelin sheath maturation (6, 60–62). TSC1/2 is capable of inhibiting Rheb, a small GTPase protein that activates mTOR (63, 64). As inhibitors of mTORC1, TSC1/2 may have a negative impact on myelination. However, loss of *Tsc1* or *Tsc2* reduces myelination in the brain during development (65, 66). In contrast, using a focal demyelination model, it was documented that the loss of *Tsc1* in adult oligodendrocyte progenitor cells increases axon remyelination and enhances myelin thickness (67). These findings suggest that TSC1/2 has different functions in developmental myelination and remyelination. In line with this, it has been proposed that mTORC1 hyperactivity in SCs delays the onset of peripheral myelination; however, if mTORC1 is hyperactivated after myelination onset, radial

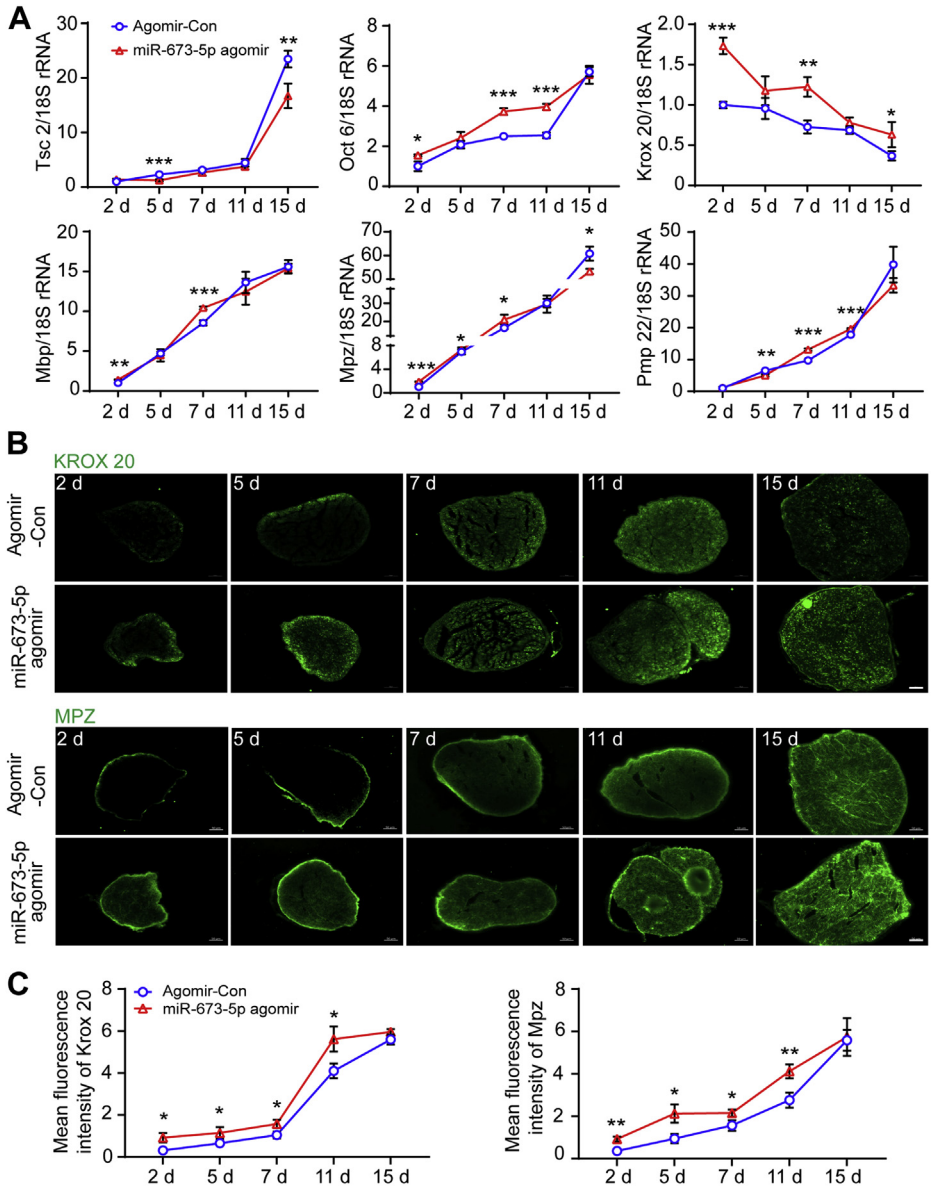

Figure 7. miRNA-673-5p antagomir stimulates myelin gene expression in newborn rat sciatic nerves. One-day old newborn rats were received miR-673-5p antagomir *via* hypodermic injection at the dosage of 5 nmol/rat every 2 days. After treatment, the sciatic nerves were collected at different time points as indicated and subjected to further analysis. *A*, *Tsc2*, *Oct6*, *Krox20*, *Mbp*, *Mpz*, and *Pmp22* expressions were analyzed by qRT-PCR. 18S rRNA was used as an internal control. *B*, the cross-sections of sciatic nerves were immunostained for Krox20 and MPZ. Scale bar = 50 μm. *C*, the fluorescent intensity for KROX20 and MPZ as shown in (*B*). Data are expressed as means ± SD. Statistical significance was analyzed by Student *t* test. $^{*}p < 0.05$, $^{**}p < 0.01$, $^{***}p < 0.001$. qRT-PCR, quantitative real-time PCR.

hypermyelination occurs (47). In the present study, we treated neonatal rats with miR-673-5p to inhibit TSC2 and observed that sciatic nerve myelination was stimulated. These results are consistent with the proposed working model of TSC1/2 in myelination, as mentioned above. Since the myelination process begins after birth (27), myelination onset in sciatic nerves should be started in 1-day-old newborn rats. At this stage, hyperactivation of mTORC1 induced by TSC2 inhibition in SCs promotes myelination.

As a downstream target of mTORC1, SREBP2 in sciatic nerves was activated by miR-673-5p. SREBP2 is a master transcriptional factor that regulates the synthesis and uptake of fatty acids and cholesterol (68). It has been shown that in the CNS, SREBP2 plays a pivotal role in myelin formation (69). Inhibition of processing SREBP2 protein reduces fatty acid and cholesterol synthesis in oligodendrocytes, which perturbs myelin formation and integrity (70). *Hmgcr* is a gene controlled by SREBP2 and plays an essential role in cholesterol biosynthesis (71). In the present study, we found that both SREBP2 and HMGCR were upregulated by miR-673-5p-induced inhibition of TSC2 in sciatic nerves. Under these conditions, the synthesis of fatty acids and cholesterol in the sciatic nerves should be enhanced. We too observed that the contents of fatty acids and cholesterol in sciatic nerves were greatly increased by miR-673-5p. These synthesized components could be used to construct the myelin sheath.

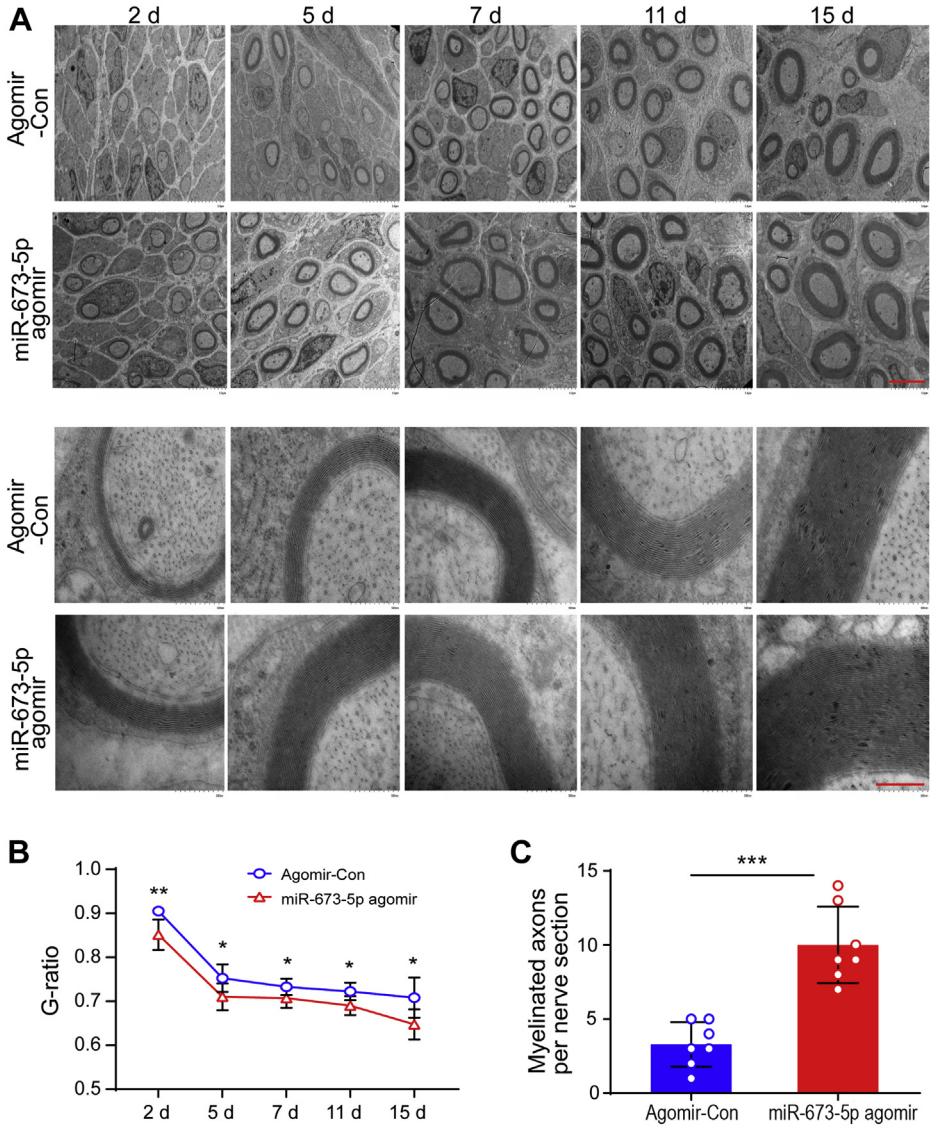

Figure 8. miRNA-673-5p antagomir promotes myelination in sciatic nerves. One-day old newborn rats were received miR-673-5p antagomir *via* hypodermic injection at the dosage of 5 nmol/rat every 2 days. The sciatic nerves were collected at different time points as indicated and subjected to further analysis. *A*, TEM images of transverse sections of sciatic nerves isolated from P2, P5, P7, P11, and P15 rats. Scale bar = 5 μm (*up panel*); Scale bar = 500 nm (*lower panel*). *B*, histogram showing average g-ratio of axons in sciatic nerves from miRNA-673-5p antagomir- and antagomir control-treated rats (n = 7). *C*, quantification of myelinated axons per nerve sections at 2 days post-miR-673-5p antagomir injection (n = 7). Data are expressed as means ± SD. Statistical significance was analyzed by Student *t* test. $*p < 0.05$, $**p < 0.01$, $***p < 0.001$. TEM, transmission electron microscopy.

Accordingly, the inhibition of AMPK stimulates protein and lipid synthesis in sciatic nerves; in this way, peripheral myelination is accelerated in newborn rats (5). *De novo* fatty acid synthesis in SCs plays an essential role in peripheral myelination (11). Furthermore, disruption of insulin signaling in SCs leads to a decline in fatty acids and cholesterol, which results in hypomyelination in the peripheral nerves (72).

Collectively, our data revealed a cross talk between fibroblasts and SCs during myelination in peripheral nerves; exosomes derived from fibroblasts were internalized by SCs and which in turn promoted myelin gene expression and myelin sheath formation. Mechanistically, exosomal miR-673-5p targets *Tsc2* and abrogates its negative regulation of mTORC1 in SCs, leading to mTORC1 activation and its downstream effectors, including *Srebp2* and *Hmgcr*. Consequently, cholesterol and lipid synthesis in SCs is stimulated, which promotes myelination in sciatic nerves. These findings unveiled an exosome-based interplay between fibroblasts and SCs in the myelination process which provided novel insights for understanding the molecular mechanisms of cholesterol and lipid biosynthesis in SCs during myelination.

Experimental procedures

Primary fibroblast culture

The sciatic nerve of 3-day-old Sprague Dawley (SD) rats were used to cultivate fibroblast cells, as described previously. Briefly, the sciatic nerves were digested with 0.125% trypsin for 30 min and 1% collagenase for 10 min at 37 °C. The cells were cultured with Dulbecco's modified Eagle's medium (DMEM)

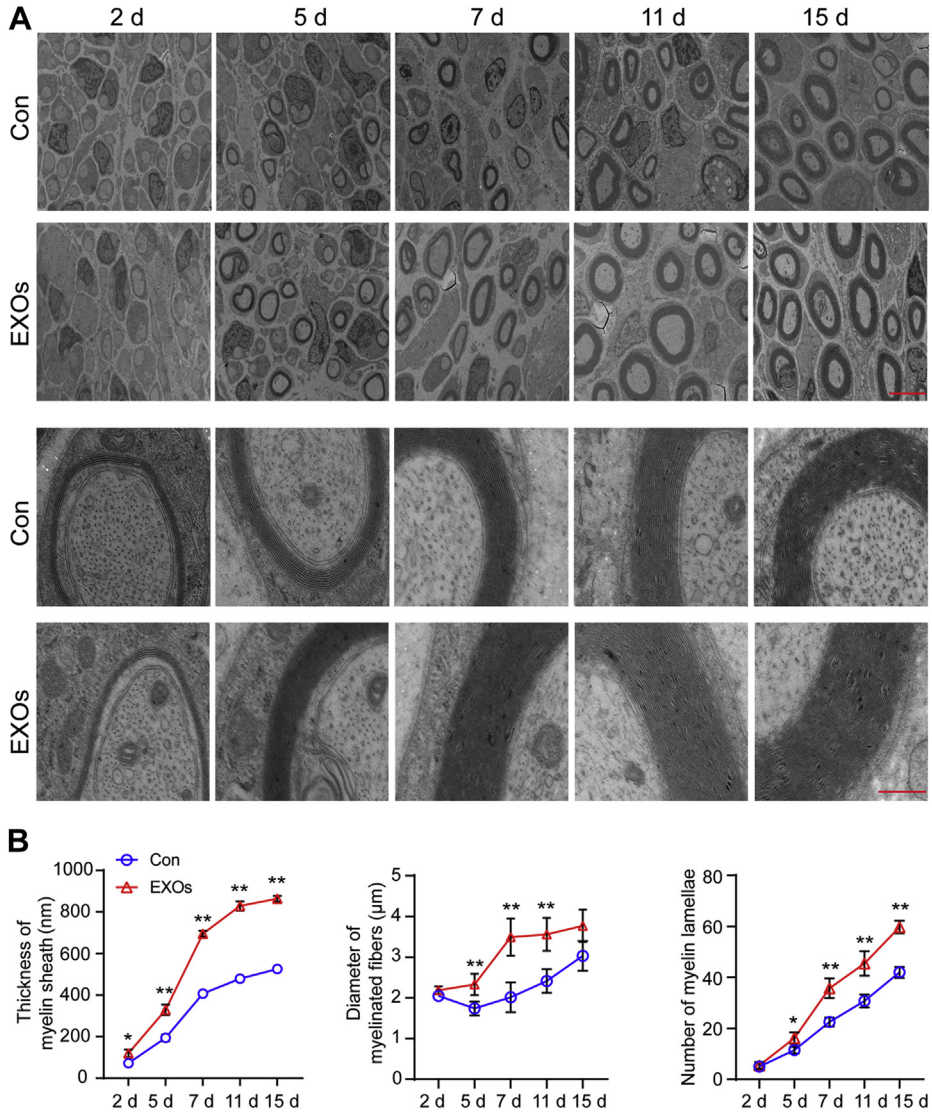

Figure 9. Fibroblast-derived exosomes promotes peripheral myelination in newborn rats. One-day old newborn rats were received 30 μl of exosomes (1.6×10^{10} particles/ml) derived from fibroblasts *via* hypodermic injection every 2 days. The sciatic nerves were collected at different time points as indicated and subjected to transmission electron microscopy (TEM) analysis. *A*, TEM images of transverse sections of sciatic nerves isolated from P2, P5, P7, P11, and P15 rats. Scale bar = 5 μm (*up panel*); Scale bar = 500 nm (*lower panel*). *B*, the thickness of myelin sheath, the diameter of myelinated fibers, and the numbers of myelin lamellae were increased by exosomes (n = 5). Data are expressed as means ± SD. Statistical significance was analyzed by Student *t* test. $^{*}p < 0.05$, $^{**}p < 0.001$. EXOs, exosomes.

medium supplemented with 10% fetal bovine serum (FBS). After 1 h, the supernatant was discarded and cultured with fresh DMEM medium supplemented with 10% FBS. Subsequently, the medium was changed every 2 days with DMEM supplemented with 10% FBS. The final preparations consisted of 98% fibroblasts, as determined by immunofluorescence for CD90.

Exosome preparation and characterization

After covering about 90% of the plate, the primary fibroblasts cells were passaged and cultured with DMEM containing 10% exosome-free FBS. The cells of passage two were used to prepare exosomes. The primary fibroblasts were cultured with DMEM basal medium for 12 h. Then, a set of cells was cultured with fresh basal medium for 12 h, and another set of cells was cultured with fresh basal medium containing 10 μM GW4869 for 12 h. After 12 h, the cell supernatant was harvest to serial centrifugations and stored at −80 °C. GW4869 is an inhibitor that can inhibit the synthesis and release of exosomes, as a control group. Ultracentrifugation was used to isolate exosomes. The cell supernatant stored at −80 °C was quickly defrosted at 37 °C. Debris and dead cells in the medium were filtrated through 0.22 μm filter. The medium was then subjected to ultracentrifugation at 100,000*g* for 2 h at 4 °C. Then washed with PBS (100,000*g* for 2 h at 4 °C), the exosome-containing pellet was resuspended in PBS. Nanoparticle tracking analysis was used to measure exosome diameter and particle number. The TEM was used to identify the morphology of the exosomes. Moreover, exosome-specific

protein markers CD9/CD63 and the negative control marker Calnexin were detected by Western blot. To monitor exosomal internalization in SCs, exosomes were labeled with PKH26 using the PKH26 fluorescent cell linker kit (Sigma-Aldrich). After PKH26 labeling, the exosomes were washed in PBS and collected by ultracentrifugation (100,000*g* for 2 h) at 4 °C. Finally, PKH26-labeled exosomes were resuspended in PBS.

Protein extraction and Western blot analysis

Protein was extracted from exosomes with a total exosome RNA and protein isolation kit (Invitrogen; Catalog No. 44-785-45). Cell lysates were centrifugated at 14,000 rpm for 10 min at 4 °C. The supernatants were collected for preparing protein samples for Western blot analysis. Protein samples were separated by SDS-PAGE and transferred to PVDF membranes. After blocking, membranes were incubated with the primary antibodies including anti-CD9 (Abcam-92726), anti-CD63 (Abcam-108950), anti-Calnexin (Abcam-133615), or anti-Actin (Abcam-179467) for overnight at 4 °C. Membranes were washed three times in Tris-buffered saline with Tween 20 and then were incubated with the second antibody for 1 h at room temperature. After further washing, chemiluminescence signals were detected with an imager system (Tanon-5200, Shanghai, China).

Culture of primary SCs

SCs were harvested from the sciatic nerves of 1-day-old SD rats, digested with trypsin and collagenase, and cultured with DMEM medium supplemented with 10% FBS. The SCs were then purified by anti-Thy 1.1 antibody and complement as described previously (73). Primary cultures of SCs were maintained in DMEM containing 10% FBS at 37 °C under humidified 5% CO_2.

Transfection

To increase expression of TSC1 and TSC2 expression in SCs, 4×10^5 cells were seeded into 6-well plates before the day for transfection. During the transfection, 1 μg of plasmid expressing *Tsc1* or *Tsc2* was mixed with Opti-MEM (Invitrogen) and Lipo8000 (Beyotimes), according to the manufacturer's instructions. The prepared mixtures were then added to each well. The plasmid expressing *Tsc1* was a gift from Cheryl Walker (Addgene plasmid #12133; http://n2t.net/addgene:12133; RRID: Addgene_12133) (74). The plasmid expressing *Tsc2* was a gift from Brendan Manning (Addgene plasmid #14129; http://n2t.net/addgene:14129; RRID: Addgene_14129) (75).

For siRNA transfection, 1 μM of *Tsc2* siRNA was transfected into SCs by electroporation with a CUY900 to 13-3-5 adherent cell electrode on an electroporation apparatus (NEPA21, Japan). The electroporation was performed two times with 50 ms interval at 50 ms pulse and 20 V. To regulate miRNA-673-5p, primary cultured SCs were transfected with miRNA-673-5p mimic or inhibitor (Ribobio) using riboFECTTM CP reagent (Ribobio) according to the manufacturer's instructions. The *Tsc2* siRNA sequences used were siRNA-1, CCA AAC AAG GCC TGA ATA A and siRNA-2, GCT GCT ACC TTG ACG AAT A.

Newborn rat treatments

miR-673-5p agomir and agomir control were synthesized at Ribobio. One-day-old newborn rats (P1) received miR-673-5p agomir *via* hypodermic injection at the dosage of 5 nmol/rat every 2 days. Control rats received the same dosage of agomir control. All animal protocols were approved by the Administration Committee of Experimental Animals, Jiangsu Province, China (Approval ID: SYXK [SU] 2017-0046).

Immunofluorescence staining

The procedures of immunofluorescence were described elsewhere (76). Briefly, cells were fixed with precooled 95% ethanol for 30 min; after rehydrating in PBS, cells were incubated in blocking solution (10% normal goat serum and 0.03 g/ml bovine serum albumin) for 1 h at 37 °C followed by incubation with primary antibodies overnight at 4 °C. The next day, after washing three times in PBS, cells were incubated with the appropriate secondary antibodies for 1 h at room temperature. To visualize the nucleus, cells were incubated with Hoechst for 10 min at room temperature. For sciatic nerves, the segments were fixed in 4% paraformaldehyde, embedded in 5% sucrose, and cut into 12-μm-thick sections on a cryostat. The prepared sections were then immunostained with primary antibodies including anti-P4HB (1:200, ab2792, Abcam), anti-fibronectin (1:200, ab2413, Abcam), anti-S100 (1:400, ab52642, Abcam), anti-Krox20 antibody (1:400, NBP2-16286, Novus), anti-Myelin Protein Zero (MPZ) antibody (1:200, ab134439, Abcam) at 4 °C for 24 h. The sections were further reacted with the FITC-labeled secondary antibody goat anti-mouse IgG (1:400, ab150117, Abcam) or the Cy3-labeled secondary antibody sheep anti rabbit IgG (1:400, ab150077, Abcam) or the 488-labeled secondary antibody goat anti-chicken IgG (1:400, ab150173, Abcam) at 4 °C overnight. Cell and tissue images were taken with a confocal laser scanning microscope (Leica).

Transmission electron microscopy

The sciatic nerve sections were fixed in 4% glutaraldehyde buffered with 0.01 M phosphate buffer and in 1% OsO_4, and then samples were dehydrated in gradient concentrations of ethanol. The samples were then embedded in Epon 812 epoxy resin, and ultrathin sections were prepared and stained with lead citrate and uranyl acetate. The slides were observed using a TEM (JEM-1230, JEOL). Images were taken from 10 random fields to determine the number of myelin sheath layers, the thickness of myelin sheaths, and the diameter of myelinated nerve fibers using Image Pro Plus software (Media Cybernetics). Mean g-ratios were calculated with a correction including nonmyelinated axons >1 μm diameter (77). For each group, at least 50 myelinated axons were included for quantification analysis.

Quantitative real-time PCR

Total RNA was extracted from cells or animal tissues using Trizol reagent (Invitrogen) and transcribed into cDNA using cDNA synthesis kit (Takara). The gene expression analysis was performed with StepOne Real-Time PCR Detection System (Applied Biosystems) with SYBR Green Supermix. The mRNA level was normalized to 18S as a house keeping gene. The primer sequences used were: 18S rRNA forward: 5′-AGT CCC TGC CCT TTG TAC ACA-3′; 18S rRNA reverse: 5′-CGT TCC GAG GGC CTC ACT-3′; *Mbp* forward: 5′-GGC ATC ACA GAA GAG ACC CTC AC-3′; *Mbp* reverse: 5′-GCC CGA TGG AGT CAA GGA TG-3′; *Mpz* forward: 5′-GGA GGC CGA GAT GCC ATT TC-3′; *Mpz* reverse: 5′-TGC CGT TGT CAC TGT AGT CTA GGTT-3′; *Oct6* forward: 5′ -TGG GCC TAG CGC ACC CTC AAT G-3′; *Oct6* reverse: 5′-GGT ACT GCC ACC GCC TGC CTT G-3′; *Pmp22* forward: 5′-ATC TCA AAG CCT TCG TCA CTC C-3′; *Pmp22* reverse: 5′-GGC CAATAC AAG TCA TCG CTA G-3′; *Krox20* forward: 5′-GAT CCT TCA GCA TTC TTA TCG-3′; *Krox20* reverse:5′-CAG GAT AGT CTG GGA TCA TAG-3′. *Tsc1* forward: 5′-TCC GTA ATA AGA GTG AGA GC-3′; *Tsc1* reverse: 5′-CTG TGT TCG TGA TGA GTC T-3′; *Tsc2* forward: 5′-ATT AAG CGT CTC CGT CAG-3′; *Tsc2* reverse: 5′-AGA GGA AAT GAG GCG TTT-3′; *Srebp 1c* forward: 5′-AGT GTT GGC CTG CTT GG-3′; *Srebp 1c* reverse: 5′-AGG TCA GCT TGT TTG CGA T-3′; *Srebp 2* forward: 5′-CTG TCG GGT GTC ATG GG-3′; *Srebp 2* reverse: 5′-GCT CGC TGT TCT CAT CCA-3′; *Fasn* forward: 5′-CCC AGA CAG AGA AGA GCC A-3′; *Fasn* reverse: 5′-CCA GCC TTC CAC CTC CT-5′; *Acly* forward: 3′-GGG AGG AAG CTG ACG AG-3′; *Acly* reverse: 5′-CCA GGG GTG ACG ATA CAG-3′; *Accl* forward: 5′-TTG GAC AAC GCC TTC AC-3′; *Accl* reverse: 5′-GCA GCC CAT TAC TTC ATC A-3′; *Hmgcr* forward: 5′-GGC TGA AGA TGT GTC CAA G-3′; *Hmgcr* reverse: 5′-AGC CAA AAG CAA CGC TAA-3′.

For miRNA detection, mature miRNAs were reversed transcribed with specific Bulge-Loop miRNA Primers using Bulge-Loop miRNA qRT-PCR Starter Kit (RiboBio). Gene expression analysis was performed with SYBR Green Supermix. mRNA level was normalized to RNU6B mature miRNA. The primers for miR-665, miR-667-3p, miR-673-5p, and miR-3072 were designed and synthesized at RiboBio. Cel-mir-39 was used as the exogenous control for miRNAs in SCs conditioned medium. Cel-miR-39 (10^9 copies/μl) was added to each sample. Total RNA was isolated from SCs conditioned medium using the exoRNeasy Kit (Qiagen).

Exosomal small RNA sequencing

The exosomal RNA was extracted with a kit for library construction and RNA-seq (Qiagen). RNA sample quality was examined by Agilent 2100 Bioanalyzer (Agilent Technologies), NanoDrop (Thermo Fisher Scientific Inc.), and electrophoresis in agrose gel. A total of 2 μg RNA was used for library construction with the NEBNext Multiplex Small RNA library Prep Set for Illumina. The sequences were processed and analyzed by GENEWIZ. First, the reads obtained by sequencing were aligned with the reference genome, regardless of the reads at multiple positions in the alignment. Then, the structure of each possible miRNA precursor was calculated with miRDeep2. According to the scoring evaluation, based on these precursor structures and scoring values, new miRNA sequences can be predicted. The transcripts per million values of the three sets of miRNA data were averaged, and the miRNAs with the mean value ≤ 10 were removed, and the expressed miRNAs were included for further analysis.

miRNA target prediction and pathway enrichment analysis

To predict potential target genes, the expressed miRNAs obtained with RNA sequencing were analyzed by the Miranda (http://www.ebi.ac.uk/ena/) and Targetscan (http://www.targetscan.org/vert_72/) software. Using currently known mammalian miRNA sequences, we scanned 3′ untranslated regions from rat (*Rattus norvegicus*) genomes for potential target sites. The scanning algorithm was based on sequence complementarity between the mature miRNA and the target site, binding energy of the miRNA–target duplex, and evolutionary conservation of the target site sequence and target position in aligned untranslated regions of homologous genes. To this end, all miRNA targets showing a conserved and a nonconserved target site were obtained. Pathway enrichment analysis was tested upon hypergeometric distribution by R 'phyper' function by using Kyoto Encyclopedia of Genes and Genomes (KEGG) database (Release 91.0). Pathways with a $p < 0.05$ were considered as significant enriched.

Protein–protein interaction network analysis

Genes related to nerve regeneration in SCs were screened for gene function enrichment analysis from GSE147285 dataset and Gene Ontology database. The interaction for each gene in the signaling pathways related to nerve regeneration in SCs and genes related to myelination were extracted based on Pathway common database (http://www.pathwaycommons.org/). Each pathway was calculated separately. The transitivity of the constructed network was calculated for measuring the possibility of adjacent nodes being connected to each other. The larger the value transitivity is, the more likely the nodes in the network exist in clusters.

KEGG pathway analysis

For KEGG pathway enrichment analysis, a rat gene database was used to map the differentially expressed genes onto pathways. Enrichment was analyzed using a hypergeometric distribution model. In hypergeometric distribution model, the candidate genes were mapped to each of the pathways. Then, a significant value (p value) was assigned to measure the significance that the genes of interest participate in a certain pathway based on hypergeometric test. The p value has been corrected using false discovery rate. The exported KEGG terms with $p < 0.05$ was regarded as statistically significant and finally selected. The total gene number represents the number of genes associated with the pathway. The Class field corresponds to the name of each KEGG pathway category.

Lipidomics analysis

Lipids were extracted by the method of methyl tert-butyl ether. Briefly, sciatic nerves were homogenized in water–methanol (1:1.2, v/v). Then methyl tert-butyl ether was added, and the mixture was ultrasound 20 min at 4 °C followed by sitting still for 30 min at room temperature. The solution was centrifuged at 14,000*g* for 15 min at 10 °C, and the upper organic solvent layer was obtained and dried under nitrogen and subjected to LC-MS/MS analysis. The dried lipid extracts were re-dissolved in 90% isopropanol/acetonitrile and centrifuged at 14,000*g* for 15 min. Lipid samples were separated by reverse phase chromatography with CSH C18 column (2.1 mm × 100 mm, Waters). Solvent A was acetonitrile–water (6:4, v/v) with 0.1% formic acid and 0.1 mM ammonium formate, and solvent B was acetonitrile–isopropanol (1:9, v/v) with 0.1% formic acid and 0.1 mM ammonium formate. Mass spectra was acquired by Q-Exactive Plus in positive and negative mode, respectively. ESI parameters were optimized and preset for all measurements as follows: source temperature, 300 °C; capillary temperature, 350 °C; the ion spray voltage was set at 3000 V; S-Lens RF level was set at 50%; and the scan range of the instruments was set at m/z 200 to 1800. Lipid species was identified by using a search engine Lipid Search (78).

Cholesterol assay

Cholesterol was extracted from the sciatic nerves with a cholesterol extraction kit (Sigma-Aldrich; MAK175). Cholesterol contents were analyzed by a kit (Sigma-Aldrich; MAK043).

Statistical analyses

Data were presented as mean ± SD. The statistical significance was analyzed by GraphPad Prism 8.0 (GraphPad Software, Inc.). The comparisons between two groups were performed using unpaired two-tailed Student's *t* test. For multiple-group comparisons, one-way ANOVA with Bonferroni's post hoc test was applied for analyzing statistical significance. $p < 0.05$ was considered statistically significant.

Data availability

The data supporting the findings of this study are included in the article and Supplementary Materials. All original data and biological resources are available from the corresponding authors upon reasonable request.

Supporting information—This article contains supporting information.

Acknowledgments—This work was provided by the National Natural Science Foundation of China (Nos. 81970747, 81701835) and the National Key Research and Development Program of China (Grant No. 2017YFA0701304).

Author contributions—C. S. and Y. Y. conceptualization; Y. Z. methodology; Y. L. and X. L. investigation; Y. Z. project administration; J. L. validation; J. M. formal analysis; J. M. data curation; Z. X. software; X. L. visualization; Y. L. writing-original draft; C. S. and Y. Y. writing-review and editing; Y. Y. Supervision; Y. Z., C. S., and Y. Y. funding acquisition.

Conflict of interest—The authors declare that they have no conflicts of interest with the contents of this article.

Abbreviations—The abbreviations used are: CNS, central nervous system; db-cAMP, dibutyryl cyclic AMP; DMEM, Dulbecco's modified Eagle's medium; FBS, fetal bovine serum; KEGG, Kyoto Encyclopedia of Genes and Genomes; mTOR, mechanistic target of the rapamycin; mTORC1, mTOR complex 1; qRT-PCR, quantitative real-time PCR; SCs, Schwann cells; SD, Sprague Dawley; SREBP, sterol-regulatory element binding protein; TEM, transmission electron microscope; TSC, tuberous sclerosis complex.

References

1. Garbay, B., Heape, A. M., Sargueil, F., and Cassagne, C. (2000) Myelin synthesis in the peripheral nervous system. *Prog. Neurobiol.* **61**, 267–304
2. Bosio, A., Binczek, E., and Stoffel, W. (1996) Functional breakdown of the lipid bilayer of the myelin membrane in central and peripheral nervous system by disrupted galactocerebroside synthesis. *Proc. Natl. Acad. Sci. U. S. A.* **93**, 13280–13285
3. Coetzee, T., Fujita, N., Dupree, J., Shi, R., Blight, A., Suzuki, K., Suzuki, K., and Popko, B. (1996) Myelination in the absence of galactocerebroside and sulfatide: Normal structure with abnormal function and regional instability. *Cell* **86**, 209–219
4. Saher, G., Brugger, B., Lappe-Siefke, C., Mobius, W., Tozawa, R., Wehr, M. C., Wieland, F., Ishibashi, S., and Nave, K. A. (2005) High cholesterol level is essential for myelin membrane growth. *Nat. Neurosci.* **8**, 468–475
5. Liu, X., Peng, S., Zhao, Y., Zhao, T., Wang, M., Luo, L., Yang, Y., and Sun, C. (2017) AMPK negatively regulates peripheral myelination *via* activation of c-jun. *Mol. Neurobiol.* **54**, 3554–3564
6. Norrmen, C., Figlia, G., Lebrun-Julien, F., Pereira, J. A., Trotzmuller, M., Kofeler, H. C., Rantanen, V., Wessig, C., van Deijk, A. L., Smit, A. B., Verheijen, M. H., Ruegg, M. A., Hall, M. N., and Suter, U. (2014) mTORC1 controls PNS myelination along the mTORC1-RXRgamma-SREBP-lipid biosynthesis axis in Schwann cells. *Cell Rep.* **9**, 646–660
7. Peterson, T. R., Sengupta, S. S., Harris, T. E., Carmack, A. E., Kang, S. A., Balderas, E., Guertin, D. A., Madden, K. L., Carpenter, A. E., Finck, B. N., and Sabatini, D. M. (2011) mTOR complex 1 regulates lipin 1 localization to control the SREBP pathway. *Cell* **146**, 408–420
8. Sawade, L., Grandi, F., Mignanelli, M., Patino-Lopez, G., Klinkert, K., Langa-Vives, F., Di Guardo, R., Echard, A., Bolino, A., and Haucke, V. (2020) Rab35-regulated lipid turnover by myotubularins represses mTORC1 activity and controls myelin growth. *Nat. Commun.* **11**, 2835
9. Dimas, P., Montani, L., Pereira, J. A., Moreno, D., Trotzmuller, M., Gerber, J., Semenkovich, C. F., Kofeler, H. C., and Suter, U. (2019) CNS myelination and remyelination depend on fatty acid synthesis by oligodendrocytes. *Elife* **8**, e44702
10. Clarke, B. A., Majumder, S., Zhu, H., Lee, Y. T., Kono, M., Li, C., Khanna, C., Blain, H., Schwartz, R., Huso, V. L., Byrnes, C., Tuymetova, G., Dunn, T. M., Allende, M. L., and Proia, R. L. (2019) The Ormdl genes regulate the sphingolipid synthesis pathway to ensure proper myelination and neurologic function in mice. *Elife* **8**, e51067
11. Montani, L., Pereira, J. A., Norrmen, C., Pohl, H. B. F., Tinelli, E., Trotzmuller, M., Figlia, G., Dimas, P., von Niederhausern, B., Schwager, R., Jessberger, S., Semenkovich, C. F., Kofeler, H. C., and Suter, U. (2018) De novo fatty acid synthesis by Schwann cells is essential for peripheral nervous system myelination. *J. Cell Biol.* **217**, 1353–1368
12. Viader, A., Sasaki, Y., Kim, S., Strickland, A., Workman, C. S., Yang, K., Gross, R. W., and Milbrandt, J. (2013) Aberrant Schwann cell lipid metabolism linked to mitochondrial deficits leads to axon degeneration and neuropathy. *Neuron* **77**, 886–898

13. LeBleu, V. S., and Neilson, E. G. (2020) Origin and functional heterogeneity of fibroblasts. *FASEB J.* **34**, 3519–3536
14. Plikus, M. V., Wang, X., Sinha, S., Forte, E., Thompson, S. M., Herzog, E. L., Driskell, R. R., Rosenthal, N., Biernaskie, J., and Horsley, V. (2021) Fibroblasts: Origins, definitions, and functions in health and disease. *Cell* **184**, 3852–3872
15. Chen, X., and Song, E. (2019) Turning foes to friends: Targeting cancer-associated fibroblasts. *Nat. Rev. Drug Discov.* **18**, 99–115
16. Mahmoudi, S., Mancini, E., Xu, L., Moore, A., Jahanbani, F., Hebestreit, K., Srinivasan, R., Li, X., Devarajan, K., Prelot, L., Ang, C. E., Shibuya, Y., Benayoun, B. A., Chang, A. L. S., Wernig, M., *et al.* (2019) Heterogeneity in old fibroblasts is linked to variability in reprogramming and wound healing. *Nature* **574**, 553–558
17. Tallquist, M. D., and Molkentin, J. D. (2017) Redefining the identity of cardiac fibroblasts. *Nat. Rev. Cardiol.* **14**, 484–491
18. Plikus, M. V., Guerrero-Juarez, C. F., Ito, M., Li, Y. R., Dedhia, P. H., Zheng, Y., Shao, M., Gay, D. L., Ramos, R., Hsi, T. C., Oh, J. W., Wang, X., Ramirez, A., Konopelski, S. E., Elzein, A., *et al.* (2017) Regeneration of fat cells from myofibroblasts during wound healing. *Science* **355**, 748–752
19. Thomas, P. K. (1963) The connective tissue of peripheral nerve: An electron microscope study. *J. Anat.* **97**, 35–44
20. Joseph, N. M., Mukouyama, Y. S., Mosher, J. T., Jaegle, M., Crone, S. A., Dormand, E. L., Lee, K. F., Meijer, D., Anderson, D. J., and Morrison, S. J. (2004) Neural crest stem cells undergo multilineage differentiation in developing peripheral nerves to generate endoneurial fibroblasts in addition to Schwann cells. *Development* **131**, 5599–5612
21. Zhang, R., Chen, S., Wang, X., Gu, X., and Yi, S. (2021) Cell populations in neonatal rat peripheral nerves identified by single-cell transcriptomics. *Glia* **69**, 765–778
22. Parrinello, S., Napoli, I., Ribeiro, S., Wingfield Digby, P., Fedorova, M., Parkinson, D. B., Doddrell, R. D., Nakayama, M., Adams, R. H., and Lloyd, A. C. (2010) EphB signaling directs peripheral nerve regeneration through Sox2-dependent Schwann cell sorting. *Cell* **143**, 145–155
23. Kalluri, R., and LeBleu, V. S. (2020) The biology, function, and biomedical applications of exosomes. *Science* **367**, eaau6977
24. Zhou, X., Brown, B. A., Siegel, A. P., El Masry, M. S., Zeng, X., Song, W., Das, A., Khandelwal, P., Clark, A., Singh, K., Guda, P. R., Gorain, M., Timsina, L., Xuan, Y., Jacobson, S. C., *et al.* (2020) Exosome-mediated crosstalk between keratinocytes and macrophages in cutaneous wound healing. *ACS Nano* **14**, 12732–12748
25. Genschmer, K. R., Russell, D. W., Lal, C., Szul, T., Bratcher, P. E., Noerager, B. D., Abdul Roda, M., Xu, X., Rezonzew, G., Viera, L., Dobosh, B. S., Margaroli, C., Abdalla, T. H., King, R. W., McNicholas, C. M., *et al.* (2019) Activated PMN exosomes: Pathogenic entities causing matrix destruction and disease in the lung. *Cell* **176**, 113–126.e15
26. Keller, M. D., Ching, K. L., Liang, F. X., Dhabaria, A., Tam, K., Ueberheide, B. M., Unutmaz, D., Torres, V. J., and Cadwell, K. (2020) Decoy exosomes provide protection against bacterial toxins. *Nature* **579**, 260–264
27. Wood, J. G., and Engel, E. L. (1976) Peripheral nerve glycoproteins and myelin fine structure during development of rat sciatic nerve. *J. Neurocytol.* **5**, 605–615
28. Zhang, Z., Yu, B., Gu, Y., Zhou, S., Qian, T., Wang, Y., Ding, G., Ding, F., and Gu, X. (2016) Fibroblast-derived tenascin-C promotes Schwann cell migration through beta1-integrin dependent pathway during peripheral nerve regeneration. *Glia* **64**, 374–385
29. van Neerven, S. G., Pannaye, P., Bozkurt, A., Van Nieuwenhoven, F., Joosten, E., Hermans, E., Taccola, G., and Deumens, R. (2013) Schwann cell migration and neurite outgrowth are influenced by media conditioned by epineurial fibroblasts. *Neuroscience* **252**, 144–153
30. Dreesmann, L., Mittnacht, U., Lietz, M., and Schlosshauer, B. (2009) Nerve fibroblast impact on Schwann cell behavior. *Eur. J. Cell Biol.* **88**, 285–300
31. Cai, S., Tsui, Y. P., Tam, K. W., Shea, G. K., Chang, R. S., Ao, Q., Shum, D. K., and Chan, Y. S. (2017) Directed differentiation of human bone marrow stromal cells to fate-committed schwann cells. *Stem Cell Rep.* **9**, 1097–1108
32. Sobue, G., and Pleasure, D. (1984) Schwann cell galactocerebroside induced by derivatives of adenosine 3',5'-monophosphate. *Science* **224**, 72–74
33. Deng, C. L., Hu, C. B., Ling, S. T., Zhao, N., Bao, L. H., Zhou, F., Xiong, Y. C., Chen, T., Sui, B. D., Yu, X. R., and Hu, C. H. (2021) Photoreceptor protection by mesenchymal stem cell transplantation identifies exosomal MiR-21 as a therapeutic for retinal degeneration. *Cell Death Differ.* **28**, 1041–1061
34. Morad, G., Carman, C. V., Hagedorn, E. J., Perlin, J. R., Zon, L. I., Mustafaoglu, N., Park, T. E., Ingber, D. E., Daisy, C. C., and Moses, M. A. (2019) Tumor-derived extracellular vesicles breach the intact blood-brain barrier *via* transcytosis. *ACS Nano* **13**, 13853–13865
35. Song, H., Li, X., Zhao, Z., Qian, J., Wang, Y., Cui, J., Weng, W., Cao, L., Chen, X., Hu, Y., and Su, J. (2019) Reversal of osteoporotic activity by endothelial cell-secreted bone targeting and biocompatible exosomes. *Nano Lett.* **19**, 3040–3048
36. Salzer, J. L. (2015) Schwann cell myelination. *Cold Spring Harb. Perspect. Biol.* **7**, a020529
37. Jeppesen, D. K., Fenix, A. M., Franklin, J. L., Higginbotham, J. N., Zhang, Q., Zimmerman, L. J., Liebler, D. C., Ping, J., Liu, Q., Evans, R., Fissell, W. H., Patton, J. G., Rome, L. H., Burnette, D. T., and Coffey, R. J. (2019) Reassessment of exosome composition. *Cell* **177**, 428–445.e18
38. Ying, W., Riopel, M., Bandyopadhyay, G., Dong, Y., Birmingham, A., Seo, J. B., Ofrecio, J. M., Wollam, J., Hernandez-Carretero, A., Fu, W., Li, P., and Olefsky, J. M. (2017) Adipose tissue macrophage-derived exosomal miRNAs can modulate *in vivo* and *in vitro* insulin sensitivity. *Cell* **171**, 372–384.e12
39. Henriques-Antunes, H., Cardoso, R. M. S., Zonari, A., Correia, J., Leal, E. C., Jimenez-Balsa, A., Lino, M. M., Barradas, A., Kostic, I., Gomes, C., Karp, J. M., Carvalho, E., and Ferreira, L. (2019) The kinetics of small extracellular vesicle delivery impacts skin tissue regeneration. *ACS Nano* **13**, 8694–8707
40. Su, T., Xiao, Y., Xiao, Y., Guo, Q., Li, C., Huang, Y., Deng, Q., Wen, J., Zhou, F., and Luo, X. H. (2019) Bone marrow mesenchymal stem cells-derived exosomal MiR-29b-3p regulates aging-associated insulin resistance. *ACS Nano* **13**, 2450–2462
41. Jiang, N., Xiang, L., He, L., Yang, G., Zheng, J., Wang, C., Zhang, Y., Wang, S., Zhou, Y., Sheu, T. J., Wu, J., Chen, K., Coelho, P. G., Tovar, N. M., Kim, S. H., *et al.* (2017) Exosomes mediate epithelium-mesenchyme crosstalk in organ development. *ACS Nano* **11**, 7736–7746
42. Thomou, T., Mori, M. A., Dreyfuss, J. M., Konishi, M., Sakaguchi, M., Wolfrum, C., Rao, T. N., Winnay, J. N., Garcia-Martin, R., Grinspoon, S. K., Gorden, P., and Kahn, C. R. (2017) Adipose-derived circulating miRNAs regulate gene expression in other tissues. *Nature* **542**, 450–455
43. Zhang, Y., Kim, M. S., Jia, B., Yan, J., Zuniga-Hertz, J. P., Han, C., and Cai, D. (2017) Hypothalamic stem cells control ageing speed partly through exosomal miRNAs. *Nature* **548**, 52–57
44. Saxton, R. A., and Sabatini, D. M. (2017) mTOR signaling in growth, metabolism, and disease. *Cell* **168**, 960–976
45. Yang, H., Rudge, D. G., Koos, J. D., Vaidialingam, B., Yang, H. J., and Pavletich, N. P. (2013) mTOR kinase structure, mechanism and regulation. *Nature* **497**, 217–223
46. Norrmen, C., Figlia, G., Pfistner, P., Pereira, J. A., Bachofner, S., and Suter, U. (2018) mTORC1 is transiently reactivated in injured nerves to promote c-Jun elevation and Schwann cell dedifferentiation. *J. Neurosci.* **38**, 4811–4828
47. Figlia, G., Norrmen, C., Pereira, J. A., Gerber, D., and Suter, U. (2017) Dual function of the PI3K-Akt-mTORC1 axis in myelination of the peripheral nervous system. *Elife* **6**, e29241
48. Furusho, M., Ishii, A., and Bansal, R. (2017) Signaling by FGF receptor 2, not FGF receptor 1, regulates myelin thickness through activation of ERK1/2-MAPK, which promotes mTORC1 activity in an Akt-independent manner. *J. Neurosci.* **37**, 2931–2946
49. Chung, J., Kuo, C. J., Crabtree, G. R., and Blenis, J. (1992) Rapamycin-FKBP specifically blocks growth-dependent activation of and signaling by the 70 kd S6 protein kinases. *Cell* **69**, 1227–1236
50. Jiang, M., Liu, L., He, X., Wang, H., Lin, W., Wang, H., Yoon, S. O., Wood, T. L., and Lu, Q. R. (2016) Regulation of PERK-eIF2alpha

signalling by tuberous sclerosis complex-1 controls homoeostasis and survival of myelinating oligodendrocytes. *Nat. Commun.* **7**, 12185
51. Yi, J., Zhu, J., Wu, J., Thompson, C. B., and Jiang, X. (2020) Oncogenic activation of PI3K-AKT-mTOR signaling suppresses ferroptosis *via* SREBP-mediated lipogenesis. *Proc. Natl. Acad. Sci. U. S. A.* **117**, 31189–31197
52. Madison, B. B. (2016) Srebp2: A master regulator of sterol and fatty acid synthesis. *J. Lipid Res.* **57**, 333–335
53. Horton, J. D., Goldstein, J. L., and Brown, M. S. (2002) SREBPs: Activators of the complete program of cholesterol and fatty acid synthesis in the liver. *J. Clin. Invest.* **109**, 1125–1131
54. Le Hellard, S., Muhleisen, T. W., Djurovic, S., Ferno, J., Ouriaghi, Z., Mattheisen, M., Vasilescu, C., Raeder, M. B., Hansen, T., Strohmaier, J., Georgi, A., Brockschmidt, F. F., Melle, I., Nenadic, I., Sauer, H., *et al.* (2010) Polymorphisms in SREBF1 and SREBF2, two antipsychotic-activated transcription factors controlling cellular lipogenesis, are associated with schizophrenia in German and Scandinavian samples. *Mol. Psychiatry* **15**, 463–472
55. Lu, X. Y., Shi, X. J., Hu, A., Wang, J. Q., Ding, Y., Jiang, W., Sun, M., Zhao, X., Luo, J., Qi, W., and Song, B. L. (2020) Feeding induces cholesterol biosynthesis *via* the mTORC1-USP20-HMGCR axis. *Nature* **588**, 479–484
56. Schmitt, S., Castelvetri, L. C., and Simons, M. (2015) Metabolism and functions of lipids in myelin. *Biochim. Biophys. Acta* **1851**, 999–1005
57. Ben-Sahra, I., Howell, J. J., Asara, J. M., and Manning, B. D. (2013) Stimulation of *de novo* pyrimidine synthesis by growth signaling through mTOR and S6K1. *Science* **339**, 1323–1328
58. Ben-Sahra, I., Hoxhaj, G., Ricoult, S. J. H., Asara, J. M., and Manning, B. D. (2016) mTORC1 induces purine synthesis through control of the mitochondrial tetrahydrofolate cycle. *Science* **351**, 728–733
59. Thoreen, C. C., Chantranupong, L., Keys, H. R., Wang, T., Gray, N. S., and Sabatini, D. M. (2012) A unifying model for mTORC1-mediated regulation of mRNA translation. *Nature* **485**, 109–113
60. Bercury, K. K., Dai, J., Sachs, H. H., Ahrendsen, J. T., Wood, T. L., and Macklin, W. B. (2014) Conditional ablation of raptor or rictor has differential impact on oligodendrocyte differentiation and CNS myelination. *J. Neurosci.* **34**, 4466–4480
61. Lebrun-Julien, F., Bachmann, L., Norrmen, C., Trotzmuller, M., Kofeler, H., Ruegg, M. A., Hall, M. N., and Suter, U. (2014) Balanced mTORC1 activity in oligodendrocytes is required for accurate CNS myelination. *J. Neurosci.* **34**, 8432–8448
62. Beirowski, B., Wong, K. M., Babetto, E., and Milbrandt, J. (2017) mTORC1 promotes proliferation of immature Schwann cells and myelin growth of differentiated Schwann cells. *Proc. Natl. Acad. Sci. U. S. A.* **114**, E4261–E4270
63. Huang, J., and Manning, B. D. (2008) The TSC1-TSC2 complex: A molecular switchboard controlling cell growth. *Biochem. J.* **412**, 179–190
64. Inoki, K., Li, Y., Xu, T., and Guan, K. L. (2003) Rheb GTPase is a direct target of TSC2 GAP activity and regulates mTOR signaling. *Genes Dev.* **17**, 1829–1834
65. Meikle, L., Talos, D. M., Onda, H., Pollizzi, K., Rotenberg, A., Sahin, M., Jensen, F. E., and Kwiatkowski, D. J. (2007) A mouse model of tuberous sclerosis: Neuronal loss of Tsc1 causes dysplastic and ectopic neurons, reduced myelination, seizure activity, and limited survival. *J. Neurosci.* **27**, 5546–5558
66. Hsieh, C. C., Lo, Y. C., Li, S. J., Lin, T. C., Chang, C. W., Chen, T. C., Yang, S. H., Lee, Y. C., and Chen, Y. Y. (2021) Detection of endophenotypes associated with neuropsychiatric deficiencies in a mouse model of tuberous sclerosis complex using diffusion tensor imaging. *Brain Pathol.* **31**, 4–19
67. McLane, L. E., Bourne, J. N., Evangelou, A. V., Khandker, L., Macklin, W. B., and Wood, T. L. (2017) Loss of tuberous sclerosis Complex1 in adult oligodendrocyte progenitor cells enhances axon remyelination and increases myelin thickness after a focal demyelination. *J. Neurosci.* **37**, 7534–7546
68. Shimano, H., and Sato, R. (2017) SREBP-regulated lipid metabolism: Convergent physiology - divergent pathophysiology. *Nat. Rev. Endocrinol.* **13**, 710–730
69. Zhou, X., Shin, S., He, C., Zhang, Q., Rasband, M. N., Ren, J., Dai, C., Zorrilla-Veloz, R. I., Shingu, T., Yuan, L., Wang, Y., Chen, Y., Lan, F., and Hu, J. (2021) Qki regulates myelinogenesis through Srebp2-dependent cholesterol biosynthesis. *Elife* **10**, e60467
70. Monnerie, H., Romer, M., Jensen, B. K., Millar, J. S., Jordan-Sciutto, K. L., Kim, S. F., and Grinspan, J. B. (2017) Reduced sterol regulatory element-binding protein (SREBP) processing through site-1 protease (S1P) inhibition alters oligodendrocyte differentiation *in vitro*. *J. Neurochem.* **140**, 53–67
71. Sharpe, L. J., Coates, H. W., and Brown, A. J. (2020) Post-translational control of the long and winding road to cholesterol. *J. Biol. Chem.* **295**, 17549–17559
72. Hackett, A. R., Strickland, A., and Milbrandt, J. (2020) Disrupting insulin signaling in Schwann cells impairs myelination and induces a sensory neuropathy. *Glia* **68**, 963–978
73. Mantuano, E., Inoue, G., Li, X., Takahashi, K., Gaultier, A., Gonias, S. L., and Campana, W. M. (2008) The hemopexin domain of matrix metalloproteinase-9 activates cell signaling and promotes migration of schwann cells by binding to low-density lipoprotein receptor-related protein. *J. Neurosci.* **28**, 11571–11582
74. Cai, S. L., Tee, A. R., Short, J. D., Bergeron, J. M., Kim, J., Shen, J., Guo, R., Johnson, C. L., Kiguchi, K., and Walker, C. L. (2006) Activity of TSC2 is inhibited by AKT-mediated phosphorylation and membrane partitioning. *J. Cell Biol.* **173**, 279–289
75. Manning, B. D., Tee, A. R., Logsdon, M. N., Blenis, J., and Cantley, L. C. (2002) Identification of the tuberous sclerosis complex-2 tumor suppressor gene product tuberin as a target of the phosphoinositide 3-kinase/akt pathway. *Mol. Cell* **10**, 151–162
76. Zhao, Y., Wang, Y., Gong, J., Yang, L., Niu, C., Ni, X., Wang, Y., Peng, S., Gu, X., Sun, C., and Yang, Y. (2017) Chitosan degradation products facilitate peripheral nerve regeneration by improving macrophage-constructed microenvironments. *Biomaterials* **134**, 64–77
77. Zhang, Y., Jiang, K., Xie, G., Ding, J., Peng, S., Liu, X., Sun, C., and Tang, X. (2021) FGF21 impedes peripheral myelin development by stimulating p38 MAPK/c-Jun axis. *J. Cell Physiol.* **236**, 1345–1361
78. Taguchi, R., and Ishikawa, M. (2010) Precise and global identification of phospholipid molecular species by an Orbitrap mass spectrometer and automated search engine Lipid Search. *J. Chromatogr. A* **1217**, 4229–4239